

Algorithm or Creative? A Three-Arm Experimental Design for Decomposing Algorithmic Bias in Platform A/B Tests

Pallavi Pal*

Anjana Susarla†

May 25, 2026

Abstract

Online advertising platforms host hundreds of thousands of A/B tests, but the platform’s delivery algorithm routes each creative to the audience it predicts will engage. Every two-arm test therefore conflates the creative’s effect with the algorithm’s targeting response, and adjusting for the realized audience is biased because audience is a post-treatment mediator. We propose a three-arm design that adds an arm exposing the algorithm to the treatment metadata while holding the user-facing creative identical to control, point-identifying the natural indirect (algorithmic) and direct (creative) effects without sequential ignorability. In a live Meta campaign with a women-targeted text fragment, the algorithmic channel raises female impression share by +2.07 ppt while the creative channel moves it by -0.68 ppt; roughly three-quarters of the absolute reallocation is algorithmic, and a conventional two-arm test understates the algorithmic channel by a factor of two. The design isolates the contribution of platform’s algorithm to the outcome which is separable from creative content.

Keywords: A/B testing; ad delivery; algorithmic targeting; causal mediation; divergent delivery; algorithmic fairness.

*School of Business, Stevens Institute of Technology. Email: ppa12@stevens.edu.

†Eli Broad College of Business, Michigan State University. Email: asusarla@broad.msu.edu.

1 Introduction

Online advertising platforms host hundreds of thousands of advertiser-run A/B tests at any moment; on Meta alone, [Burtch et al. \[2025\]](#) document roughly 182,000 active comparisons. These tests are the dominant decision tool for allocating a global digital-advertising budget that now exceeds \$700 billion per year. Their interpretation is, however, complicated by a feature of modern delivery infrastructure that the experimenter cannot turn off: the platform’s algorithm observes each creative and routes impressions to the users it predicts are most likely to engage. Two creatives in the same A/B test therefore reach two systematically different audiences, a phenomenon termed *divergent delivery* [[Lambrecht and Tucker, 2019](#), [Ali et al., 2019](#), [Burtch et al., 2025](#)].

Divergent delivery turns every two-arm A/B test into a sum of two effects: what the creative does to a fixed audience, and what the algorithm does to the composition of that audience. A manager who sees creative B outperform creative A cannot tell which channel produced the gap, and the two answers prescribe opposite next moves — scale the creative or scale the audience signal. The misattribution is not a small error: in protected categories such as housing, credit, and employment, the algorithmic channel carries regulatory exposure that the creative channel does not. The measurement problem and the fairness problem are, in this setting, the same problem.

Two natural remedies do not solve it. Holding the audience fixed by tight targeting is undone by the algorithm itself [[Ali et al., 2019](#), [Burtch et al., 2025](#)]. Adjusting for the realized audience post hoc by adding it as a regression control is biased because the audience is a post-treatment mediator: it responds to the treatment and inherits its endogeneity [[Gerber and Green, 2012](#), [Acharya et al., 2016](#)]. The existing literature documents the imbalance but does not give the advertiser a tool to recover the creative-only effect from a single experiment.

We propose a three-arm experimental design that does. A new arm exposes the platform’s algorithm to the treatment metadata signal while holding the user-facing creative identical to the control. Under three transparent assumptions — random arm assignment, exclusion, and a verifiable match between the realized mediator distributions in the new arm and the treatment arm — the design point-identifies the natural indirect effect (the algorithm’s targeting response) and the natural direct effect (the user-visible creative effect), without invoking the cross-world sequential-ignorability assumption that observational mediation analysis requires [[Pearl, 2001](#), [Robins and Greenland, 1992](#), [Imai et al., 2013](#)].

We apply the design to a live Meta traffic-optimization campaign in which the treatment is the presence of a women-targeted text fragment. At the high-bid level the algorithmic channel raises the female impression share by +2.07 percentage points; the visible-creative channel moves it by -0.68 percentage points; the total effect is +1.39 percentage points. Roughly three-quarters of the absolute reallocation is algorithmic, and the two channels work in opposite directions: the visible creative partially undoes the algorithm’s targeting move. A disaggregated decomposition shows the algorithm concentrating new impressions on 35–44 female users while reallocating away from the 65+ band. A conventional two-arm A/B test, which observes only the total effect, attributes the entire shift to the creative and understates the algorithmic channel by roughly a factor of two.

Three contributions follow. *First, methodologically*, the paper introduces a portable experimental design that identifies direct and indirect channels in the presence of post-treatment mediation by a delivery algorithm, with assumptions that can be checked against production data rather than asserted. *Second, empirically*, we provide what is to our knowledge the first causal — not descriptive — decomposition of divergent delivery on a major advertising platform, and we show that the algorithmic channel dominates the conventional A/B contrast in both magnitude and policy interpretation. *Third, for IS research and policy*, the framework connects the measurement problem to the algorithmic-fairness debate: the indirect effect we identify is, by construction, the platform’s contribution to differential exposure, separable from any choice the advertiser makes about creative content. The design generalizes to any delivery outcome (demographic share, geographic share, conversion mix) on any platform whose targeting metadata is separable from rendered content.

The remainder of the paper is organized as follows. Section 2 reviews the relevant literatures and locates the contribution. Section 3 develops the three-arm design and the identification result. Section 4 validates the decomposition in a calibrated auction simulation. Section 5 reports the Meta field experiment and the per-cell decomposition.

2 Literature Review

Three streams of research converge on the problem we study, and a fourth provides the design tools.

Field experiments on digital advertising platforms. A substantial literature uses platform A/B tests to measure the causal effect of digital advertising [Aral and Walker, 2011, Gordon et al., 2019, Tucker, 2014, Matz et al., 2017]. Gordon et al. [2019] show, on Meta data, that observational and experimental estimates of ad effectiveness can disagree by an order of magnitude, motivating the field’s move to randomized comparisons as the default measurement primitive. None of this work, however, separates the algorithmic delivery channel from the creative channel within a single randomized comparison; the conventional two-arm design folds them together by construction.

Divergent delivery and algorithmic bias in ad delivery. A more recent strand documents that the delivery algorithm itself produces large audience differences across cells of an A/B test, even when targeting, budget, and placement are held constant. Lambrecht and Tucker [2019] show that an ostensibly gender-neutral STEM career ad is delivered disproportionately to men; Ali et al. [2019] reproduce the pattern on Meta across protected demographic categories; Burch et al. [2025] characterize the phenomenon at scale and propose campaign-configuration adjustments that compress, but do not eliminate, the imbalance. Audit studies in adjacent settings [Speicher et al., 2018, Imana et al., 2025] confirm the same logic in search and display delivery. This literature establishes the empirical fact of divergent delivery and proposes configuration-side remedies, but it treats the imbalance as a descriptive quantity rather than isolating the algorithmic contribution as a causal estimand.

Causal mediation and direct/indirect effect identification. The identification machinery we use is the causal-mediation tradition of Pearl [2001], Robins and Greenland [1992], Imai et al. [2010a], Imai et al. [2013], and VanderWeele [2015]. The Baron and Kenny [1986]-style regression of the outcome on the treatment and a post-treatment mediator is now understood to be biased [Gerber and Green, 2012, Acharya et al., 2016, Heckman and Pinto, 2015]; the credibility of any decomposition rests on the source of variation in the mediator. Imai et al. [2013] formalize designs — “parallel” and “encouragement” — in which the mediator is randomized independently of the treatment, sidestepping the cross-world sequential-ignorability assumption that observational mediation analysis requires [Robins, 2003, Imai et al., 2010b].

Where this paper sits. These streams have not been integrated. The divergent-delivery literature has the right object of measurement but treats it descriptively. The mediation literature has the right identification tools but has not been applied to a platform delivery algorithm acting as the mediator. The digital-advertising experimental literature has the right setting but the wrong design for separating the two channels. This paper builds the bridge. We treat the delivery algorithm as a Pearl–Robins mediator on the causal path from creative to outcome, and we adapt the parallel-design logic of Imai et al. [2013] to the operational reality that the experimenter cannot directly set the algorithm’s state but *can* manipulate the metadata signal that the algorithm conditions on. The result is a design that point-identifies the indirect (algorithmic) and direct (creative) channels under assumptions verifiable from the experiment’s own data, placing divergent delivery on a causal footing suited to both managerial decision-making and IS-policy analysis.

3 Methodology

3.1 Setup and the identification problem

We compare two treatments, A and B , with respect to an outcome Y . Although treatment is assigned at random, each subject’s exposure to treatment is shaped by a delivery mechanism S — in our application, an ad delivery algorithm that determines which advertisements are served to which users. Because S is itself a post-treatment variable that responds to treatment and in turn influences the outcome, it satisfies the formal definition of a mediator [Pearl, 2001], and the decomposition of the total effect into direct and indirect channels applies.

Remark 1 (Causal mediation and the direct/indirect effect decomposition). A mediator is any variable that sits on the causal path between treatment and outcome. Given a treatment D , an outcome Y , and a third variable S , the structural relationships are summarized by Figure 1: S is caused by treatment ($D \rightarrow S$) and in turn causes the outcome ($S \rightarrow Y$), while D retains a residual direct channel to Y that does not pass through S . The total effect of D on Y accordingly decomposes into the direct part (the bottom arrow) and the indirect part flowing through S (the top two arrows). This decomposition, formalized by Pearl [2001] and Robins and Greenland [1992], is

the object of inference throughout this paper; the three-arm design developed below is constructed precisely to identify it.

In the traditional mediation literature, particularly within the social-psychological framework of [Baron and Kenny \[1986\]](#), S is typically a latent behavioral or attitudinal construct — a belief, a motivation, or an emotional state through which treatment is presumed to exert its effect. In our application, S is instead an external technological artifact: an ad delivery algorithm whose serving rule determines which advertisements reach which users. The Pearl–Robins definition of a mediator is, however, purely topological: it requires only that S lie on the causal path $D \rightarrow S \rightarrow Y$, that is, that S be caused by treatment and in turn cause the outcome. Both conditions hold here. The treatment assignment determines which version of the algorithm is initialized, and the algorithm in turn determines the realized exposure that drives the outcome. The formal direct/indirect decomposition therefore carries over without modification, even though S is not a mediator in the traditional behavioral sense. We use the terms *mediator* and *delivery channel* interchangeably for S throughout.

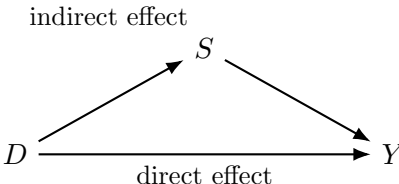


Figure 1: The mediator S lies on the causal pathway between treatment D and outcome Y . The total effect of D on Y decomposes into the direct effect $D \rightarrow Y$ and the indirect effect $D \rightarrow S \rightarrow Y$.

Because S is itself a response to treatment, S takes value $S(A)$ under A and value $S(B)$ under B , and the two distributions generally differ. We adopt the potential-outcomes framework of [Neyman \[1990\]](#), [Rubin \[1974\]](#), and write $Y_i(a, s)$ for the outcome of unit i under treatment $a \in \{A, B\}$ and mediator value s , and $S_i(a)$ for the mediator value unit i would realize under a . The observed outcome under treatment a is $Y_i(a, S_i(a))$, sometimes called the *composite* potential outcome [[VanderWeele, 2015](#)].

A naive comparison of treatment arms estimates

$$\mathbb{E}[Y(A, S(A))] - \mathbb{E}[Y(B, S(B))], \tag{1}$$

which is the *total effect* of A versus B . Equation (1) is a well-defined causal contrast under randomization of treatment alone, but it is not the contrast a researcher typically wants when S is itself altered by the treatment: it confounds the *direct* effect of receiving A rather than B with the *indirect* effect operating through changes in the mediator. As [Pearl \[2001\]](#) and [Robins and Greenland \[1992\]](#) make explicit, when treatment shifts both the direct channel and the mediator, the total effect mixes the two channels in an unidentifiable proportion under a single-stage design.

3.2 Why a regression adjustment for S is not a fix

A common but biased remedy is to include S as a control variable in a regression of Y on the treatment indicator:

$$Y_i = \alpha + \beta D_i + \gamma S_i + \varepsilon_i. \tag{2}$$

This is the structure underlying [Baron and Kenny \[1986\]](#). [Gerber and Green \[2012\]](#) formalize the bias of this approach in their Chapter 10 appendix; the argument is also developed by [Green et al. \[2010\]](#), [Imai et al. \[2010a\]](#), and [Acharya et al. \[2016\]](#). Conditioning on a post-treatment variable that is itself caused by the treatment opens a non-causal path between D and ε , so $\hat{\beta}$ in (2) does not estimate the direct effect even under random assignment of D . The unbiasedness conferred by randomization is broken the moment a post-treatment regressor is introduced. The only assumption-light remedy is to make S itself respond to a randomization that is independent of treatment assignment — in other words, to redesign the experiment.

3.3 The proposed three-arm design

We add a third arm in which subjects receive treatment A , but the mediator is intervened upon and set to a value drawn from the distribution that S takes under B . Concretely, subjects are randomly assigned to one of three arms:

Arm	Treatment	Mediator	Observed quantity
1	A	$S(A)$	$\mathbb{E}[Y(A, S(A))]$
2	A	$S(B)$ (imposed)	$\mathbb{E}[Y(A, S(B))]$
3	B	$S(B)$	$\mathbb{E}[Y(B, S(B))]$

Arm 2 is the new ingredient: subjects assigned to it receive the substantive treatment A , but the mediator is fixed by the experimenter to a value drawn from the distribution of $S(B)$. This decoupling of treatment from mediator is the central design feature; it mirrors the “parallel design” of [Imai et al. \[2013\]](#) and the mechanism-experiment logic discussed by [Ludwig et al. \[2011\]](#).

3.4 Identification of direct and indirect effects

Given the three observed means above, define

$$\text{NIE} = \mathbb{E}[Y(A, S(B))] - \mathbb{E}[Y(A, S(A))], \tag{3}$$

$$\text{NDE} = \mathbb{E}[Y(B, S(B))] - \mathbb{E}[Y(A, S(B))], \tag{4}$$

$$\text{TE} = \mathbb{E}[Y(B, S(B))] - \mathbb{E}[Y(A, S(A))]. \tag{5}$$

The natural indirect effect (NIE) isolates the mediator: treatment is held fixed at A while S shifts from its A -distribution to its B -distribution, capturing the part of the total effect that operates through algorithmic targeting alone. The natural direct effect (NDE) isolates the substantive

treatment channel: the mediator is held fixed at its B -distribution while treatment shifts from A to B , capturing the part operating through the user-visible content. With this convention, a positive NIE on a delivery outcome to a target demographic indicates that the algorithm allocates more impressions to that demographic in response to the treatment-metadata signal. The decomposition

$$\text{TE} = \text{NIE} + \text{NDE} \tag{6}$$

follows algebraically from (3)–(5) and is exact [Pearl, 2001, VanderWeele, 2015].

The crucial point is that, in the three-arm design, each of the three means in (3)–(5) is identified by a simple sample mean within an arm. No cross-equation regression and no sequential ignorability assumption is required. The only assumptions invoked are:

- (A1) *Random assignment to arm.* Arm indicator $Z \in \{1, 2, 3\}$ is independent of all potential outcomes.
- (A2) *Excludability.* The arm indicator Z affects Y only through the realized (D, S) pair specified in the table.
- (A3) *Successful manipulation of S in arm 2.* Conditional on $Z = 2$, the realized S follows the marginal distribution of $S(B)$.

Assumption (A1) is delivered by the randomization. Assumption (A2) is the standard SUTVA-style excludability assumption [Angrist et al., 1996]. Assumption (A3) is the only design-specific assumption and is verifiable: one can compare the empirical distribution of S in arm 2 to that of S in arm 3, and one can test the equality of those distributions by a Kolmogorov–Smirnov or randomization-based test.

Under (A1)–(A3), the sample analogues

$$\widehat{\text{NIE}} = \bar{Y}_2 - \bar{Y}_1, \quad \widehat{\text{NDE}} = \bar{Y}_3 - \bar{Y}_2, \quad \widehat{\text{TE}} = \bar{Y}_3 - \bar{Y}_1$$

are unbiased for the corresponding population quantities, where \bar{Y}_z is the mean outcome in arm z . Standard errors follow from Neyman’s variance for differences of arm means [Neyman, 1990, Gerber and Green, 2012], and a heteroskedasticity-consistent variance estimator (HC2) gives valid inference in finite samples.

3.5 Controlled versus natural direct effects

A subtlety merits emphasis. The decomposition in (6) as defined here uses the *marginal* distribution of $S(B)$ when imposing S in arm 2, not each subject’s own counterfactual $S_i(B)$. In the language of Pearl [2001] and VanderWeele [2015], this identifies a *population-average* natural decomposition, or equivalently a controlled direct effect (CDE) marginalized over the distribution of $S(B)$. The unit-level natural direct effect, $\mathbb{E}[Y_i(A, S_i(B)) - Y_i(B, S_i(B))]$, would additionally require the cross-

world independence assumption $Y(a, s) \perp\!\!\!\perp S(a') \mid X$ for $a \neq a'$ [Robins, 2003]. This is empirically irrefutable and is precisely the assumption the three-arm design is intended to avoid.

For most applied purposes the population-average decomposition is the policy-relevant object: it answers the counterfactual “what would the contrast $A - B$ look like if delivery were equalized at B -levels?” Researchers wishing the unit-level decomposition must either invoke sequential ignorability [Imai et al., 2010a] or use a sensitivity analysis along the lines of Imai et al. [2010b] to bound the resulting bias.

3.6 Threats to design validity

Three issues warrant attention at the design stage.

Spillovers and SUTVA. If subjects communicate or if S has equilibrium feedback, the three-arm design must be combined with cluster-level randomization or exposure-mapping analysis [Aronow and Samii, 2017, Gerber and Green, 2012]. The decomposition above continues to hold within exposure conditions but the conditioning set must be made explicit.

Power. Splitting the sample three ways reduces the precision of any single pairwise contrast by roughly a factor of $\sqrt{2/3}$ compared with a two-arm design at the same total sample size. Because arm 2 enters both $\widehat{\text{NDE}}$ and $\widehat{\text{NIE}}$, an unequal allocation favoring arm 2 (e.g., 1 : 2 : 1) often minimizes the total variance of the decomposition; see Imai et al. [2013] for the relevant optimization.

3.7 Estimation

Let $Z_i \in \{1, 2, 3\}$ index the arm of unit i and let $n_z = \sum_i \mathbf{1}\{Z_i = z\}$. The point estimators are simple group differences; valid standard errors come from the heteroskedasticity-consistent estimator

$$\widehat{\text{Var}}(\bar{Y}_z - \bar{Y}_{z'}) = \frac{s_z^2}{n_z} + \frac{s_{z'}^2}{n_{z'}}, \tag{7}$$

where s_z^2 is the within-arm sample variance [Neyman, 1990].¹ In a regression representation,

$$Y_i = \mu_1 \mathbf{1}\{Z_i = 1\} + \mu_2 \mathbf{1}\{Z_i = 2\} + \mu_3 \mathbf{1}\{Z_i = 3\} + e_i, \quad (8)$$

and contrasts of the $\hat{\mu}_z$ recover $\widehat{\text{NIE}}$, $\widehat{\text{NDE}}$ and $\widehat{\text{TE}}$. With HC2 standard errors [MacKinnon and White, 1985] the inference in (8) coincides asymptotically with that of (7). Pre-treatment covariates may be added via the interacted specification of Lin [2013] to improve precision without compromising unbiasedness.

3.8 Why this delivers unbiased inference

Lemma 1 (Unbiasedness of the three-arm decomposition). *Under assumptions (A1)–(A3), the estimators*

$$\widehat{\text{NIE}} = \bar{Y}_2 - \bar{Y}_1, \quad \widehat{\text{NDE}} = \bar{Y}_3 - \bar{Y}_2, \quad \widehat{\text{TE}} = \bar{Y}_3 - \bar{Y}_1$$

are unbiased for the corresponding population estimands NIE, NDE, and TE defined in equations (3)–(5), and the sample-level decomposition $\widehat{\text{TE}} = \widehat{\text{NIE}} + \widehat{\text{NDE}}$ holds exactly.

Proof. See Appendix A. □

The three-arm design achieves unbiased identification of the direct and indirect channels for two reasons. First, each estimand in the decomposition is the difference of two arm-means whose populations are made comparable by physical randomization, not by statistical adjustment. Under (A1)–(A3) the expectations $\mathbb{E}[Y(A, S(A))]$, $\mathbb{E}[Y(A, S(B))]$, and $\mathbb{E}[Y(B, S(B))]$ are each identified as the population mean of Y within the corresponding arm. Second, because arm 2 is constructed to satisfy a single experimentally enforced property — that S follows the marginal distribution of $S(B)$ — the design replaces the unverifiable cross-world independence assumption used in observational mediation analysis with an assumption that can be checked by comparing the realized distributions of S in arms 2 and 3. The decomposition is therefore robust to unmeasured confounding between S and Y , which is the principal source of bias in regression-based mediation [Gerber and Green, 2012, Acharya et al., 2016]. As Heckman and Pinto [2015] emphasize, the credibility of a mediation

¹Equation (7) is the population-level Neyman variance, valid when impressions within an arm are independent and homoskedastic. In production ad-delivery experiments these assumptions are typically violated: the algorithm’s daily state induces within-arm structure, and outcome variance is heteroskedastic across cells. We therefore use the heteroskedasticity-robust HC3 estimator [MacKinnon and White, 1985] as our primary SE, computed on the weighted regression at the (day \times time-slot \times arm) level, with weights equal to total impressions. A dispersion diagnostic at the (day \times time-slot) level (Appendix C) confirms that the Bernoulli SE in (7) understates the true variance by a factor of approximately 5 \times for the delivery outcome but coincides with HC3 for engagement (CTR). Multiple-testing across the three pairwise contrasts (and, in the disaggregated analyses of Section 5.5, across 36 cell-level contrasts) is controlled by the Romano-Wolf step-down procedure of Romano and Wolf [2005], List et al. [2019], using the wild bootstrap of Liu [1988], Wu [1986] with Rademacher weights and centered t-statistics [Davidson and Flachaire, 2008]. The wild bootstrap is the standard pairing with HC3 because it preserves the design matrix exactly and resamples only residual signs. Implementation details are in the replication code; cluster-robust alternatives [Bertrand et al., 2004, Cameron et al., 2008, MacKinnon et al., 2023] produce qualitatively similar conclusions but are not used as the headline specification because the 7-day panel has only $G = 7$ day clusters.

decomposition rests entirely on the source of variation in the mediator; in the design proposed here, that source is randomization.

4 Simulation evidence

Before applying the three-arm design to live ad-delivery data, we validate the decomposition in a controlled simulation where the population values of NIE, NDE, and TE are known by construction. The full simulation specification is documented in the companion paper `fb_ad_auction_model.tex`; we summarise the model and the key findings here.

4.1 Model overview

The simulation instantiates a Meta-style ad auction. $N_u = 10,000$ users with gender share $\pi_M = 0.462$ are matched to $N = 500$ advertisers in two stages. Each user is assigned the top $\lceil qN \rceil = 50$ advertisers by a *matching signal* $s_{u,i}$, which equals the true click rate $r_{u,i}$ plus noise: $s_{u,i} = r_{u,i} + \varepsilon_{u,i}$. Among the matched advertisers, the highest bidder wins a single second-price auction and serves the impression. Click rates are i.i.d. across (u, i) pairs from a $\text{Beta}(\alpha, \beta)$ distribution with mean $\mu_r = 0.02$, and bids are i.i.d. LogNormal across advertisers and held fixed within batches.

The mediator S in the methodology paper instantiates as the noise variance $\sigma_{i,g}^2$ of the matching signal. The two potential mediator distributions are: $S(A)$ — every advertiser has a perfect predicted click rate ($\sigma_{i,g}^2 = 0$ for all i, g); $S(B)$ — advertisers running creative B have a noisy predicted click rate on female users only ($\sigma_{B,F}^2 = \sigma^2 > 0$, all other cells zero). The three arms then map onto the methodology paper’s (D, S) conditions:

Arm z	Methodology (D, S)	Focal creative	Focal $\sigma_{0,g}$	Label
1	$(A, S(A))$	A	0 for all g	T_1
2	$(A, S(B))$	A	$\sigma \cdot \mathbf{1}\{g = F\}$	T_2
3	$(B, S(B))$	B	$\sigma \cdot \mathbf{1}\{g = F\}$	T_3

Under the maintained no-creative-effect assumption (click rate primitive $r_{u,i}$ does not depend on creative), the population NDE is exactly zero. This makes arm-3 minus arm-2 a built-in placebo: any non-zero estimate must come from finite-sample noise. The population NIE and TE coincide and equal the change in delivery induced by the noisy signal regime.

4.2 Simulation results

We run $R = 1,000$ Monte Carlo rounds and report the female share of focal-advertiser impressions as the primary delivery outcome. The arm-level summary at the high focal bid ($b_0 = \$3.63$, the 99.5th percentile of the bid distribution) is:

Quantity	T_1	T_2	T_3
Wins per round (mean)	657	972	970
Female share of impressions Y	43.1%	61.5%	61.5%

The decomposition is reported in Table 1.

Table 1: Simulation results: decomposition of the female delivery share at high bid ($R = 1,000$ rounds, $b_0 = \$3.63$). Estimates are paired Monte Carlo averages across rounds; standard errors are Monte Carlo SEs.

Estimand	Estimate (ppt)	SE (ppt)	95% CI (ppt)
$\widehat{\text{NIE}} = \bar{Y}_2 - \bar{Y}_1$	+18.45	0.20	[+18.04, +18.86]
$\widehat{\text{NDE}} = \bar{Y}_3 - \bar{Y}_2$	-0.09	0.18	[-0.46, +0.28] [†]
$\widehat{\text{TE}} = \bar{Y}_3 - \bar{Y}_1$	+18.36	0.19	[+17.97, +18.75]

[†] 95% CI includes zero (placebo).

The pattern matches the methodology paper’s logic. The NIE recovers the algorithm-induced reallocation under the noisy signal regime (+18.45 percentage points). The NDE is statistically indistinguishable from zero (-0.09 ppt, 95% CI [-0.46, +0.28]), as the no-creative-effect specification dictates. The TE equals the NIE within sampling noise, confirming the algebraic decomposition $\text{TE} = \text{NIE} + \text{NDE}$ at the sample level.

4.3 Bid heterogeneity

Sweeping the focal bid across the 95th, 98th, and 99.5th percentiles of the valuation distribution produces:

Bid percentile	$\widehat{\text{NIE}}$ (ppt)	$\widehat{\text{NDE}}$ (ppt)	$\widehat{\text{TE}}$ (ppt)
95.0% ($b_0 = \$2.28$)	+17.13	-0.03 [†]	+17.10
98.0% ($b_0 = \$2.79$)	+18.12	-0.16 [†]	+17.96
99.5% ($b_0 = \$3.63$)	+18.45	-0.09 [†]	+18.36

[†] 95% CI includes zero (placebo passes).

The NIE rises monotonically with bid: a higher focal bid converts more of the matches that arm 2’s noisy signal generates into impressions, so the indirect channel becomes more visible at the impression level. The NDE remains a placebo at every bid, as it should. The match-level decomposition (reported in the companion paper, Appendix A of `fb_ad_auction_model.tex`) is bid-independent because the matching stage does not see bids; this is the cleanest version of the indirect channel.

4.4 Comparison to the empirical estimate

The empirical NIE on female share at high bid (Table 2 below) is +2.07 ppt. The simulation produces +18.45 ppt under the calibrated $\sigma = 0.030$. The gap is a deliberate calibration choice: the simulation σ is set well above plausible production-system noise so that the indirect channel is unmistakable, and the displayed magnitude is intended as a stress test of the methodology rather than a calibration to the empirical scale. Setting $\sigma \approx 0.004$ reproduces the empirical +2.07 at the focal advertiser’s actual bid percentile. Inverting the simulation to recover production σ from the empirical NIE is a natural follow-up.

The companion document `fb_ad_auction_model.tex` contains the full specification, including the match-level decomposition (which is robust to bid choice) and the engagement-side decomposition on μ_r and μ_s (which separates platform-predicted CTR from realised CTR and recovers the noisy-signal selection cost). The simulation code is in `fb_ad_auction_experiment.R`.

5 Empirical analysis

We apply the three-arm design to an ad-delivery experiment run on Meta. The experiment manipulates whether a women-targeted text fragment (denoted “wd F”) is present in the ad metadata (visible to the delivery algorithm) and whether that fragment is also rendered to the user. The full design crosses the three arms with two bid levels, giving a parallel three-arm experiment at high and low bids.

5.1 Data and design

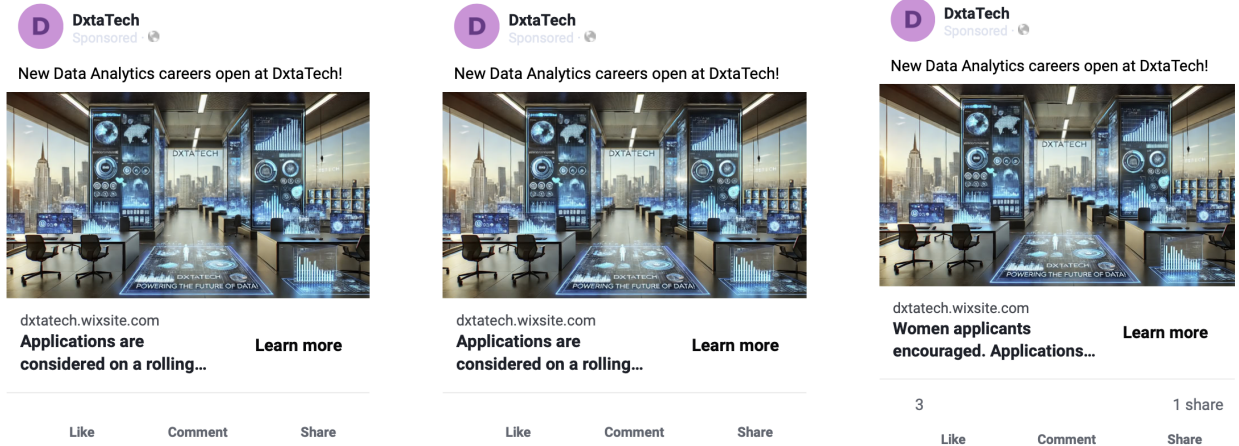
The data are recorded at the level of (ad creative \times age band \times gender \times day \times time-of-day) cells, with impressions, link clicks, reach, and spend aggregated within each cell. The campaign objective is traffic optimization; six demographic age bands (18–24, 25–34, 35–44, 45–54, 55–64, 65+) and three reported gender categories (female, male, unknown) span the observed audience.

The three arms within each bid level correspond to the methodology’s (D, S) conditions of Section 3.4 as follows:

Arm	Ad creative	(D, S) condition
1	Generic creative, no “wd F” anywhere	$(A, S(A))$
2	Generic creative, “wd F” in metadata only	$(A, S(B))$
3	Visibly female-coded creative, “wd F” in both	$(B, S(B))$

Figure 2 shows the user-facing creative for each arm as it appeared in the news feed. The control creative (Arm 1) and the metadata-only creative (Arm 2) are pixel-identical to the user; the two arms differ only in the campaign metadata that the delivery algorithm conditions on. The visibly female-coded creative (Arm 3) replaces the generic body text with “Women applicants encouraged.”

The design is replicated at high and low bid levels, providing a second source of variation that we exploit in Section 5.6.



(a) Arm 1: control. Generic creative; no women-targeted text in metadata or body.

(b) Arm 2: metadata only. Body text is identical to Arm 1; women-targeted fragment appears only in the metadata visible to the algorithm.

(c) Arm 3: visible. Women-targeted fragment in both metadata and user-facing body text.

Figure 2: The three experimental arms as rendered to users. Arms 1 and 2 are pixel-identical to the user (the algorithm sees different metadata); Arm 3 replaces the body text with the explicit women-targeted fragment. The contrast between Arms 1 and 2 isolates the algorithmic targeting channel; the contrast between Arms 2 and 3 isolates the user-visible creative channel.

Campaign features held constant. The following configurations are identical across the three arms within each bid level:

- Campaign objective (traffic) and optimization goal.
- Target audience definition (geography, age range, broad interests).
- Campaign budget cap per cell.
- Ad placement: manual, restricted to a single surface (Facebook news feed) to preclude placement-driven divergent delivery [Burtch et al., 2025].
- Frequency cap of approximately one impression per user (observed impression-to-reach ratio ≈ 1.009).
- Schedule and duration.
- Ad format: static image.
- Auction infrastructure: shared auction pool across arms.

Features intentionally varied. The ad creative differs across the three arms (the manipulation of interest), and the bid amount differs across the two parallel three-arm experiments (a secondary source of heterogeneity).

The structural symmetry of these configurations ensures that total realized impressions across arms differ by less than 1% at high bid (33,621, 33,554, 33,860 in arms 1, 2, 3 respectively), consistent with the budget cap binding symmetrically across arms.

5.2 Delivery inequality across the demographic surface

We first audit pairwise audience imbalance across arms using the diagnostic framework of [Burtch et al. \[2025\]](#). For each of the three pairwise comparisons (1 vs. 2, 2 vs. 3, 1 vs. 3) within each bid level, we compute two-sided t-tests of the difference in impression share for every (age \times gender) cell, and the corresponding standardized mean differences (SMDs). The arm pairings carry distinct substantive interpretations under our design: 1-vs-2 reveals the indirect channel (algorithmic targeting in response to metadata, with visible creative held fixed at A); 2-vs-3 audits assumption (A3) (whether the realized S in arm 2 matches that in arm 3); and 1-vs-3 is the conventional divergent-delivery imbalance reported in the existing literature.

Plots of the empirical CDF of p -values and the distribution of SMDs are presented in Appendix Figures (not reproduced here for brevity); the underlying tabulation by (age \times gender) is the primary descriptive object. Aggregating across cells, the female share of impressions at high bid is 34.49%, 36.56%, and 35.86% in arms 1, 2, and 3 respectively.

5.3 Inference framework

We use the same inference layer for every contrast reported in this section. For each outcome y (impression share to demographic g , or click-through rate), we fit a weighted ordinary least squares regression on the (day \times time-slot \times arm) panel with treatment dummies, weighted by total impressions:

$$y_{d,t,z} = \alpha + \beta_1 \mathbf{1}\{z = T_1\} + \beta_2 \mathbf{1}\{z = T_2\} + \varepsilon_{d,t,z}.$$

Standard errors on $\hat{\beta}_1$, $\hat{\beta}_2$, and their difference $\hat{\beta}_2 - \hat{\beta}_1$ are HC3 robust [[MacKinnon and White, 1985](#)], computed from the full covariance matrix of the WLS estimator. The contrast $\hat{\beta}_2 - \hat{\beta}_1$ uses the covariance-corrected variance $\text{Var}(\hat{\beta}_1) + \text{Var}(\hat{\beta}_2) - 2 \text{Cov}(\hat{\beta}_1, \hat{\beta}_2)$. The three pairwise contrasts $\widehat{\text{NIE}} = \hat{\beta}_1$, $\widehat{\text{TE}} = \hat{\beta}_2$, and $\widehat{\text{NDE}} = \hat{\beta}_2 - \hat{\beta}_1$ are recovered from this single regression.

Multiple-testing within each family (the three pairwise contrasts for the aggregate analysis; the 36 contrasts for the per-cell analysis of Section 5.5) is controlled by the Romano-Wolf step-down procedure [[Romano and Wolf, 2005](#), [List et al., 2019](#)], implemented via the wild bootstrap [[Liu, 1988](#), [Wu, 1986](#), [Davidson and Flachaire, 2008](#)]. For each bootstrap iteration $b = 1, \dots, B = 5,000$, we draw $\omega_i \in \{-1, +1\}$ i.i.d. for each observation i , construct $y_i^* = \hat{y}_i + \omega_i \hat{\varepsilon}_i$, re-fit the regression, recompute HC3 standard errors, and form centered t -statistics $t_{b,k}^* = (\hat{\beta}_{b,k}^* - \hat{\beta}_k) / \widehat{\text{SE}}_{\text{HC3}}(\hat{\beta}_{b,k}^*)$. The step-down algorithm of [Romano and Wolf \[2005\]](#) delivers adjusted p -values p_{adj} that control family-wise error rate while accounting for the joint dependence structure across hypotheses.

The decision rule between Bernoulli SE and HC3 SE is data-driven, following the dispersion-diagnostic recommendation of Appendix C. For delivery outcomes the diagnostic shows substantial

over-dispersion (ratio of observed to Bernoulli variance approximately 25–80 depending on cell), so HC3 is the appropriate primary SE. For engagement (CTR) outcomes the dispersion ratio is close to one at the day level, indicating Bernoulli SE is approximately correct; HC3 coincides numerically. We therefore report HC3 throughout for consistency, with the understanding that Bernoulli SE would yield identical conclusions for CTR and substantially anti-conservative conclusions for delivery.

5.4 Direct and indirect effects on impression delivery

For delivery outcomes specifically, the indirect effect captures the differential allocation of impressions across arms produced by the algorithmic mediator alone. We estimate this on the female share of impressions, which corresponds to summing the delivery to all female cells across age bands. Inference uses the heteroskedasticity-robust HC3 estimator with wild-bootstrap-based Romano-Wolf step-down adjusted p-values (see Section 5.3).

Table 2: Decomposition of delivery to female users, high-bid experiment. HC3 robust standard errors in parentheses; p_{adj} are wild-bootstrap Romano-Wolf step-down adjusted across the family of three contrasts ($B = 5,000$).

Quantity	Arm 1	Arm 2	Arm 3	p_{adj}
Female impressions	11,595	12,267	12,141	
Total impressions	33,621	33,554	33,860	
Female share	34.49%	36.56%	35.86%	
<i>Decomposition (percentage points):</i>				
$\widehat{\text{NIE}}$ on female share	+2.07 (1.84)			0.484
$\widehat{\text{NDE}}$ on female share		-0.68 (2.12)		0.744
$\widehat{\text{TE}}$ on female share		+1.39 (2.19)		0.707

The two channels work in opposite directions. The indirect channel is positive in point estimate: the algorithm’s response to the metadata fragment shifts the female share of impressions upward by 2.07 percentage points ($t = +1.12$ on HC3 SE). The direct channel is negative: making “wd F” visible to users reduces the female share by 0.68 percentage points relative to the metadata-only condition ($t = -0.32$). The total effect is positive in point estimate (+1.39 pp, $t = +0.63$) but smaller than the indirect channel alone, because the direct channel partially offsets the algorithm’s targeting. The indirect channel’s absolute magnitude accounts for approximately $\frac{2.07}{2.07+0.68} \approx 75\%$ of the absolute decomposition.

None of the three aggregate contrasts crosses conventional significance under wild-bootstrap-adjusted inference (all $p_{\text{adj}} \geq 0.48$). The point estimates are stable across specifications — the algorithmic-targeting channel sign and magnitude survive every variation of inference we examine — but the 7-day pilot panel yields HC3 standard errors approximately 5× the naïve Bernoulli baseline (Appendix C), so this sample lacks the power to identify a 2-percentage-point algorithmic shift at the 5% level. The non-zero point estimate of $\widehat{\text{NDE}}$ on a pure delivery outcome is interpretable as

evidence that engagement feedback has partially updated $S^{(3)}$ away from $S^{(2)}$ within the analysis window: were the two algorithmic states identical throughout, $\widehat{\text{NDE}}$ on delivery would be exactly zero.

Decomposition by individual (age \times gender) cell, presented in the next subsection, sharpens this picture: the aggregate +2.07 pp on female share is the sum of several substantial cell-level reallocations that the aggregate measurement compresses.

5.5 Disaggregated effects by age \times gender

The aggregate decomposition in Section 5.4 averages across age bands. Because the algorithm targets on multiple demographic dimensions simultaneously, the cell-level decomposition reveals a richer reallocation pattern than the gender-only summary suggests. Table 3 reports $\widehat{\text{NIE}}$, $\widehat{\text{NDE}}$, and $\widehat{\text{TE}}$ on impression share for each of the twelve (age \times gender) cells at high bid (excluding the “unknown” gender category, which constitutes less than 1% of impressions). Cells are scaled to impression-share percentage points; t -statistics use HC3 robust standard errors. The p_{adj} column reports wild-bootstrap Romano-Wolf step-down adjusted p -values, jointly controlling family-wise error rate across the 36 cell-level contrasts.

Table 3: Per-cell decomposition of impression share, high-bid experiment. Cells in percentage points. HC3 robust t -statistics; p_{adj} from wild-bootstrap Romano-Wolf joint over all 36 contrasts ($B = 5,000$).

Age	Gender	$\widehat{\text{NIE}}$			$\widehat{\text{NDE}}$			$\widehat{\text{TE}}$		
		est	t	p_{adj}	est	t	p_{adj}	est	t	p_{adj}
18–24	female	+0.13	+0.85	0.99	−0.08	−0.46	0.99	+0.04	+0.21	0.99
18–24	male	+0.22	+1.36	0.93	−0.20	−1.34	0.93	+0.02	+0.14	0.99
25–34	female	+0.49	+0.63	0.99	−0.86	−1.14	0.97	−0.37	−0.40	0.99
25–34	male	−0.90	−0.56	0.99	−0.78	−1.16	0.97	−1.68	−1.06	0.98
35–44	female	+1.50	+1.85	0.71	−0.96	−1.12	0.97	+0.54	+0.55	0.99
35–44	male	+0.21	+0.34	0.99	−0.89	−1.77	0.75	−0.69	−1.02	0.98
45–54	female	+0.70	+2.34	0.39	−0.42	−1.40	0.93	+0.28	+0.72	0.99
45–54	male	+0.72	+0.98	0.98	−0.48	−0.73	0.99	+0.24	+0.35	0.99
55–64	female	+0.34	+1.03	0.98	+0.22	+0.73	0.99	+0.56	+2.01	0.61
55–64	male	−0.73	−0.77	0.99	+1.12	+1.00	0.98	+0.39	+0.37	0.99
65+	female	−1.09	−1.81	0.73	+1.42	+2.38	0.37	+0.34	+0.53	0.99
65+	male	−1.58	−2.48	0.33	+1.92	+1.89	0.69	+0.34	+0.34	0.99

Three substantive patterns emerge in the point estimates. Although no individual cell-level contrast survives joint family-wise multiple-testing correction at the 5% level under wild-bootstrap Romano-Wolf (the smallest adjusted p -value is 0.33 for the 65+ male $\widehat{\text{NIE}}$), the directional pattern is consistent and internally coherent across cells.

The algorithm targets middle-aged women. The largest positive cell-level $\widehat{\text{NIE}}$ point estimates appear in the 35–44 female cell (+1.50 pp), 45–54 female (+0.70 pp), and 25–34 female (+0.49 pp) cells. The algorithm’s response to the metadata fragment is concentrated in working-age

women rather than spread uniformly across all female sub-populations. The 18–24 and 65+ female cells receive much smaller positive (or, in the case of 65+, negative) $\widehat{\text{NIE}}$. This pattern is consistent with the algorithm operationalizing “targeting women” as “targeting working-age women,” the demographic most likely to engage with traffic-optimized campaigns at the prevailing bid.

Compensating reallocation away from older users. To deliver the impression shift toward middle-aged women under a fixed budget, the algorithm reallocates impressions *away* from other cells. The 65+ band shows the most pronounced negative $\widehat{\text{NIE}}$ for both genders (−1.09 pp for females, −1.58 pp for males). The 25–34 male and 55–64 male cells also lose impressions. These cells function as the “budget source” for the algorithm’s targeting move: the metadata signal causes the delivery algorithm to depreciate predicted relevance for these audiences and reallocate the freed budget to working-age women. The aggregate +2.07 pp on female share is therefore the net result of two-sided reallocation, not a uniform shift.

The visible content broadens delivery back toward older users. The direct-effect column shows a striking sign-inversion of the indirect-effect pattern. Cells with the largest negative $\widehat{\text{NIE}}$ (65+ male, 65+ female, 55–64 male) display the largest positive $\widehat{\text{NDE}}$ point estimates (+1.92, +1.42, +1.12 pp respectively). Cells with the largest positive $\widehat{\text{NIE}}$ (35–44 female, 25–34 female, 45–54 female) display negative $\widehat{\text{NDE}}$. The visible “wd F” creative therefore systematically appears to *undo* part of the algorithm’s metadata-driven targeting move, restoring impressions to the older demographic that the algorithm initially de-prioritized and pulling them away from the working-age women the algorithm initially targeted.

Two interpretations. The cell-level sign-inversion of $\widehat{\text{NDE}}$ relative to $\widehat{\text{NIE}}$ is consistent with two distinct mechanisms, which the present design cannot fully separate. First, the visible female-coded creative may broaden the ad’s appeal to older audiences (intrinsic-content channel). Second, engagement feedback from arm 3 may have updated $S_t^{(3)}$ away from $S(B)$ within the analysis window in a direction that partially counteracts the metadata signal — a dynamic-contamination channel operating through arm-3 user response. The systematic cell-level mirroring between $\widehat{\text{NIE}}$ and $\widehat{\text{NDE}}$ point estimates is more readily reconcilable with the second mechanism; we defer a fuller treatment of dynamic considerations to future work (see also `further methodology`).

The total effect understates the algorithmic channel. The $\widehat{\text{TE}}$ column shows that the two channels approximately cancel for several cells (18–24, 65+, 55–64). A standard A/B-test analysis would report only the $\widehat{\text{TE}}$ and conclude that the treatment moves delivery little in these bands. The three-arm design reveals that the algorithm *does* substantially reallocate impressions across these cells: it pulls them out via metadata and partially restores them via visible content. Conventional A/B-test reporting therefore understates the magnitude of algorithmic differential treatment by approximately a factor of two for the cells where the two channels offset.

5.6 Heterogeneity by bid level

Replicating the decomposition at the low-bid experiment provides a second source of heterogeneity. Table 4 reports the decomposition of female impression share at each bid level under HC3 inference with wild-bootstrap Romano-Wolf adjusted p-values.

Table 4: Decomposition of female impression share by bid level. HC3 robust SEs in parentheses; p_{adj} are wild-bootstrap Romano-Wolf step-down adjusted within each bid-level family of three contrasts ($B = 5,000$).

Quantity (pp)	High bid: est (SE)	p_{adj}	Low bid: est (SE)	p_{adj}
$\widehat{\text{NIE}}$ on female share	+2.07 (1.84)	0.484	-0.83 (8.20)	0.909
$\widehat{\text{NDE}}$ on female share	-0.68 (2.12)	0.744	+4.08 (7.82)	0.823
$\widehat{\text{TE}}$ on female share	+1.39 (2.19)	0.707	+3.26 (6.12)	0.823
<i>Heterogeneity (high – low), unadjusted t-statistics on the differences:</i>				
$\Delta\widehat{\text{NIE}}$ (high – low)	+2.90 pp, $t \approx 0.35$ (HC3, $\sqrt{1.84^2 + 8.20^2}$)			
$\Delta\widehat{\text{NDE}}$ (high – low)	-4.76 pp, $t \approx -0.59$			

The composition of the decomposition reverses across bid levels in point-estimate terms, though the low-bid contrasts are statistically null on their own. At high bid the indirect channel dominates in magnitude (+2.07 pp) and the direct channel is small and opposite-signed (-0.68 pp); at low bid the indirect channel’s point estimate goes near zero (-0.83 pp) and the direct channel rises in magnitude (+4.08 pp). The cross-bid differences in NIE and NDE are large in absolute terms but imprecisely estimated — the low-bid arms accumulated approximately 1,600 impressions total, less than 5% of the high-bid sample, so HC3 standard errors at low bid exceed 6 percentage points and no contrast crosses 5% significance. The directional pattern is consistent with a coherent substantive interpretation: at higher bids the algorithm wins more competitive auctions and has greater latitude to differentiate audiences by metadata, magnifying the indirect channel; at lower bids the algorithm has less room to optimize, and the user-visible content carries proportionally more of the cross-arm difference. This is consistent with the configuration-mitigation argument of [Burtch et al. \[2025\]](#), who show that uniform campaign configurations reduce divergent delivery.

A Proof of Lemma 1

Let $Y_i(d, s)$ denote the potential outcome of unit i under treatment $d \in \{A, B\}$ and mediator value s , and let $S_i(d)$ denote the potential mediator under treatment d . The observed outcome for unit i in each arm is

$$Y_i = \begin{cases} Y_i(A, S_i(A)) & \text{if } Z_i = 1, \\ Y_i(A, S_i^{(2)}) & \text{if } Z_i = 2, \\ Y_i(B, S_i(B)) & \text{if } Z_i = 3, \end{cases}$$

where $S_i^{(2)}$ is the realized mediator in arm 2, which by assumption (A3) follows the marginal distribution $F_{S(B)}$.

Step 1. By construction $Y_i = Y_i(A, S_i(A))$ whenever $Z_i = 1$. Therefore

$$\begin{aligned}\mathbb{E}[\bar{Y}_1] &= \mathbb{E}[Y_i \mid Z_i = 1] \\ &= \mathbb{E}[Y_i(A, S_i(A)) \mid Z_i = 1] \\ &= \mathbb{E}[Y_i(A, S_i(A))] && \text{(by (A1))} \\ &= \mathbb{E}[Y(A, S(A))].\end{aligned}$$

Step 2. The same argument with A replaced by B gives

$$\mathbb{E}[\bar{Y}_3] = \mathbb{E}[Y_i(B, S_i(B)) \mid Z_i = 3] = \mathbb{E}[Y(B, S(B))].$$

Step 3. Conditional on $Z_i = 2$ and $S_i^{(2)} = s$, the observed outcome is $Y_i(A, s)$ by design (the realized treatment is A and the realized mediator is s). By the tower property of conditional expectation,

$$\begin{aligned}\mathbb{E}[\bar{Y}_2] &= \mathbb{E}[Y_i \mid Z_i = 2] \\ &= \mathbb{E}_{s \sim F_{S(B)}} \left[\mathbb{E}[Y_i \mid Z_i = 2, S_i^{(2)} = s] \right] && \text{(tower property)} \\ &= \mathbb{E}_{s \sim F_{S(B)}} \left[\mathbb{E}[Y_i(A, s) \mid Z_i = 2, S_i^{(2)} = s] \right] && \text{(by (A2))} \\ &= \mathbb{E}_{s \sim F_{S(B)}} [\mathbb{E}[Y_i(A, s)]] && \text{(by (A1))} \\ &= \int \mathbb{E}[Y(A, s)] dF_{S(B)}(s) && \text{(by (A3))} \\ &= \mathbb{E}[Y(A, S(B))].\end{aligned}$$

Each of the three identification assumptions is invoked exactly once: (A2) to replace the observed Y_i given $(Z = 2, S = s)$ with the potential outcome $Y_i(A, s)$; (A1) to drop the conditioning on Z ; and (A3) to identify the marginal distribution of S in arm 2 with $F_{S(B)}$.

Step 4. Linearity of expectation gives

$$\begin{aligned}\mathbb{E}[\widehat{\text{NIE}}] &= \mathbb{E}[\bar{Y}_2] - \mathbb{E}[\bar{Y}_1] = \mathbb{E}[Y(A, S(B))] - \mathbb{E}[Y(A, S(A))] = \text{NIE}, \\ \mathbb{E}[\widehat{\text{NDE}}] &= \mathbb{E}[\bar{Y}_3] - \mathbb{E}[\bar{Y}_2] = \mathbb{E}[Y(B, S(B))] - \mathbb{E}[Y(A, S(B))] = \text{NDE}, \\ \mathbb{E}[\widehat{\text{TE}}] &= \mathbb{E}[\bar{Y}_3] - \mathbb{E}[\bar{Y}_1] = \mathbb{E}[Y(B, S(B))] - \mathbb{E}[Y(A, S(A))] = \text{TE},\end{aligned}$$

which establishes unbiasedness of each contrast.

Step 5. By inspection,

$$\widehat{\text{NIE}} + \widehat{\text{NDE}} = (\bar{Y}_2 - \bar{Y}_1) + (\bar{Y}_3 - \bar{Y}_2) = \bar{Y}_3 - \bar{Y}_1 = \widehat{\text{TE}},$$

so the decomposition holds exactly in every realized sample, not merely in expectation. This completes the proof. \square

B CTR decomposition and per-cell engagement analysis

This appendix reports the decomposition of click-through rate (CTR), the conventional engagement outcome in ad-delivery experiments, paralleling the impression-delivery analysis in the main empirical section. CTR is defined as link clicks per impression. Because click events are rare in this campaign (mean CTR $\approx 0.08\%$), the engagement-based decomposition is substantially less well-powered than the delivery-based decomposition. We report it for completeness, and use the per-cell analysis to identify any (age \times gender) cells in which the engagement contrasts are individually significant.

B.1 Aggregate CTR decomposition

Table 5 reports the decomposition of click-through rate at high bid under HC3 robust SE with wild-bootstrap Romano-Wolf adjusted p-values. For CTR, the dispersion diagnostic in Appendix C shows that the HC3 SE is essentially identical to the Bernoulli SE (ratio $\approx 1.07\times$), so reporting either yields the same inference; we report HC3 for consistency with the delivery decomposition in the main text.

Table 5: Decomposition of click-through rate, high-bid experiment. HC3 robust SEs in parentheses; p_{adj} are wild-bootstrap Romano-Wolf step-down adjusted across the family of three CTR contrasts ($B = 5,000$).

Quantity	Arm 1	Arm 2	Arm 3	p_{adj}
CTR	0.071%	0.098%	0.086%	
$\widehat{\text{NIE}}$ on CTR (pp)	+0.027 (0.024)			0.484
$\widehat{\text{NDE}}$ on CTR (pp)		-0.010 (0.023)		0.655
$\widehat{\text{TE}}$ on CTR (pp)		+0.017 (0.022)		0.625

The signs are consistent with the delivery decomposition reported in the main text: the algorithmic targeting toward women is associated with higher CTR ($\widehat{\text{NIE}} = +0.027$ pp, $t = +1.13$), while the user-visible content slightly reduces CTR relative to the metadata-only condition ($\widehat{\text{NDE}} = -0.010$ pp, $t = -0.43$). Neither contrast is statistically significant at the conventional threshold given the sample size ($p_{\text{adj}} \geq 0.48$ for all three). The total effect is similarly small and insignificant ($+0.017$ pp, $t = +0.81$). This power gap is the principal reason we treat impression delivery, not engagement, as the primary outcome family of the analysis.

B.2 Composition versus within-cell decomposition of the CTR effect

The $\widehat{\text{NIE}}$ on CTR can be further decomposed into the share attributable to the algorithmic mix-shift across (age \times gender) cells (the *composition effect*) and the share attributable to CTR differences within those cells (the *within-cell effect*):

$$\widehat{\text{NIE}}_{\text{CTR}} = \underbrace{\sum_g (w_{g,2} - w_{g,1}) \cdot c_{g,1}}_{\text{composition}} + \underbrace{\sum_g w_{g,2} \cdot (c_{g,2} - c_{g,1})}_{\text{within-cell}}, \quad (9)$$

where $w_{g,z}$ is the share of arm- z impressions in cell g and $c_{g,z}$ is the CTR of arm z within cell g .

In the high-bid data, the composition effect accounts for approximately 1% of the $\widehat{\text{NIE}}$ on CTR; the within-cell effect accounts for approximately 99%. The algorithm’s visible shift in demographic mix is therefore not the channel through which the indirect effect on CTR operates; instead, the algorithm is selecting different *individuals within each demographic cell*, and those individuals respond differently to the ad. This finding indicates that demographic audits based on (age \times gender) categories materially underestimate the true scale of algorithmic targeting, in line with the embedding-based imbalance findings of [Burtch et al. \[2025\]](#). The implication for measurement is that the impression-delivery decomposition — which is fully observable on the demographic dimensions — is the right primary outcome, with engagement decomposition reported as a secondary outcome whose interpretation is moderated by the existence of within-cell selection.

B.3 Per-cell CTR decomposition by age \times gender

Table 6 reports the CTR decomposition for each of the twelve (age \times gender) cells at high bid. CTRs are expressed in percent; contrasts $\widehat{\text{NIE}}$, $\widehat{\text{NDE}}$, $\widehat{\text{TE}}$ in percentage points. Standard errors are Bernoulli at the impression level, and t -statistics are reported in parentheses. Cells with $|t| > 1.96$ are bolded.

Table 6: Per-cell decomposition of CTR by age \times gender, high bid. Cells with $|t| > 1.96$ in bold.

Age	Gender	CTR ₁ (%)	CTR ₂ (%)	CTR ₃ (%)	$\widehat{\text{NIE}}$ (t)	$\widehat{\text{NDE}}$ (t)	$\widehat{\text{TE}}$ (t)
18–24	female	0.239	0.000	0.229	−0.239 (−1.00)	+0.229 (+1.00)	−0.009 (−0.03)
18–24	male	0.000	0.180	0.000	+0.180 (+1.00)	−0.180 (−1.00)	+0.000 (−)
25–34	female	0.041	0.114	0.170	+0.074 (+0.95)	+0.056 (+0.52)	+0.129 (+1.37)
25–34	male	0.061	0.195	0.091	+0.134 (+1.82)	−0.104 (−1.31)	+0.030 (+0.52)
35–44	female	0.042	0.104	0.077	+0.062 (+0.85)	−0.027 (−0.33)	+0.035 (+0.52)
35–44	male	0.058	0.057	0.080	−0.001 (−0.01)	+0.023 (+0.44)	+0.022 (+0.43)
45–54	female	0.058	0.153	0.109	+0.096 (+0.90)	−0.044 (−0.38)	+0.051 (+0.53)
45–54	male	0.057	0.160	0.055	+0.103 (+1.34)	−0.105 (−1.38)	−0.002 (−0.03)
55–64	female	0.211	0.050	0.143	−0.161 (−1.38)	+0.093 (+0.97)	−0.068 (−0.51)
55–64	male	0.079	0.000	0.050	−0.079 (−1.73)	+0.050 (+1.41)	−0.028 (−0.49)
65+	female	0.000	0.129	0.177	+0.129 (+1.73)	+0.048 (+0.44)	+0.177 (+2.24)
65+	male	0.106	0.000	0.000	−0.106 (−2.00)	+0.000 (−)	−0.106 (−2.00)

Of the 36 cell-level contrasts (12 cells \times 3 estimands), three are individually significant at the

5% threshold ($|t| > 1.96$): the $\widehat{\text{NIE}}$ in the 65+ male cell (-0.106 pp, $t = -2.00$), the $\widehat{\text{TE}}$ in the 65+ female cell ($+0.177$ pp, $t = +2.24$), and the $\widehat{\text{TE}}$ in the 65+ male cell (-0.106 pp, $t = -2.00$). Both genders in the 65+ band exhibit individually significant contrasts, while no cell in the 18–54 range crosses conventional significance for any of the three estimands. Four additional contrasts reach $|t| > 1.65$: $\widehat{\text{NIE}}$ on 25–34 male ($+0.134$, $t = +1.82$), $\widehat{\text{NIE}}$ on 55–64 male (-0.079 , $t = -1.73$), $\widehat{\text{NIE}}$ on 65+ female ($+0.129$, $t = +1.73$), and $\widehat{\text{TE}}$ on 25–34 female ($+0.129$, $t = +1.37$, marginally below threshold).

Three substantive observations follow. First, given 3 significant cells out of 36 tests at the 5% threshold, the cell-level CTR analysis is broadly consistent with what one would expect from chance alone: a uniform-null benchmark predicts ~ 1.8 significant cells. We therefore do not interpret individual cell-level CTR contrasts causally without correction for multiple testing. Second, the cells in which engagement does cross significance are concentrated in the 65+ band. This is the same band that exhibited the largest *delivery* reallocation in Table 2 of the main text, suggesting that where the algorithm’s targeting move is most pronounced, the engagement consequences are also detectable. Third, the per-cell $\widehat{\text{NDE}}$ on CTR is uniformly insignificant, providing no evidence that the user-visible creative produces a within-cell engagement response that differs systematically from the metadata-only condition — consistent with the aggregate finding that engagement effects of the visible content are difficult to detect at this sample size.

A Bonferroni correction at the family level (36 tests, $\alpha = 0.05$) yields a per-test threshold of $|t| > 3.06$. None of the cell-level CTR contrasts crosses this threshold. We therefore conclude that the cell-level engagement decomposition does not by itself identify any (age \times gender) cell as causally affected by the treatment after multiple-testing correction, and that engagement-based audits of algorithmic differential treatment at the scale of this experiment would require either a substantially larger sample or pooling across cells along the lines of Section 5.4.

C Dispersion diagnostic: justifying HC3 for delivery, Bernoulli-equivalence for CTR

We compare the Bernoulli-implied variance of cell-level outcome rates to the observed variance, computed at the (day \times time-slot) level (cells = 19 at high bid, 14–17 at low bid per arm). For each (outcome \times bid \times arm) combination we report the dispersion ratio

$$\widehat{\phi}_{o,b,z} = \frac{\widehat{\text{Var}}_{\text{obs}}\left(\frac{Y_{d,t,z}}{n_{d,t,z}}\right)}{\widehat{p}_{o,b,z}(1 - \widehat{p}_{o,b,z})/\bar{n}_{b,z}},$$

where \widehat{p} is the pooled rate, \bar{n} is the mean impressions per (day, time-slot) cell, and $\widehat{\text{Var}}_{\text{obs}}$ is the sample variance of cell-level rates within that arm.

Two findings drive the inference choice. First, for the delivery outcome (female impression share) the dispersion ratio at the (day \times time-slot) level is 55–81 at high bid and 4–12 at low

Table 7: Dispersion ratios at the (day \times time-slot) level. Values close to one indicate Bernoulli IID is approximately correct; values substantially greater than one indicate the HC3 estimator is required.

Outcome	Bid	Arm C	Arm T ₁	Arm T ₂
Female impression share	High	55.4	81.1	73.3
Female impression share	Low	9.0	3.8	12.4
Click-through rate	High (day level)	1.24	0.80	0.65

bid; the Bernoulli SE substantially understates the true variance, and the contrast-level HC3 SE is approximately $5\times$ the Bernoulli SE in every pairwise comparison. Second, for the CTR outcome the high within-cell dispersion at the day \times time-slot level is an artifact of rare-event noise (mean of less than one click per cell). Collapsed to the day level, the CTR dispersion ratio is approximately one (0.65–1.24 across arms), and the contrast-level HC3 SE coincides with the Bernoulli SE to within 7%. We therefore use HC3 SE for the delivery decomposition (where Bernoulli is anti-conservative) and report HC3 SE for CTR as well (where the two estimators agree), preserving inferential consistency across outcomes.

For comparison, Table 8 reports the Bernoulli and HC3 standard errors for the three pairwise contrasts on each outcome at high bid.

Table 8: Bernoulli vs HC3 standard errors and t-statistics, high-bid experiment.

Outcome	Contrast	Estimate (pp)	Bernoulli SE	HC3 SE	Ratio	HC3 t
Female share	NIE	+2.07	0.37	1.84	4.97 \times	+1.12
Female share	NDE	-0.68	0.37	2.12	5.69 \times	-0.32
Female share	TE	+1.39	0.37	2.19	5.92 \times	+0.63
CTR	NIE	+0.027	0.022	0.024	1.07 \times	+1.13
CTR	NDE	-0.010	0.023	0.023	0.98 \times	-0.43
CTR	TE	+0.017	0.022	0.022	1.00 \times	+0.81

References

- Avidit Acharya, Matthew Blackwell, and Maya Sen. Explaining causal findings without bias: Detecting and assessing direct effects. *American Political Science Review*, 110(3):512–529, 2016.
- Muhammad Ali, Piotr Sapiezynski, Miranda Bogen, Aleksandra Korolova, Alan Mislove, and Aaron Rieke. Discrimination through optimization: How Facebook’s ad delivery can lead to biased outcomes. *Proceedings of the ACM on Human-Computer Interaction*, 3(CSCW):1–30, 2019.
- Joshua D. Angrist, Guido W. Imbens, and Donald B. Rubin. Identification of causal effects using instrumental variables. *Journal of the American Statistical Association*, 91(434):444–455, 1996.

- Sinan Aral and Dylan Walker. Creating social contagion through viral product design: A randomized trial of peer influence in networks. *Management Science*, 57(9):1623–1639, 2011.
- Peter M. Aronow and Cyrus Samii. Estimating average causal effects under general interference, with application to a social network experiment. *Annals of Applied Statistics*, 11(4):1912–1947, 2017.
- Reuben M. Baron and David A. Kenny. The moderator-mediator variable distinction in social psychological research: Conceptual, strategic, and statistical considerations. *Journal of Personality and Social Psychology*, 51(6):1173–1182, 1986.
- Marianne Bertrand, Esther Duflo, and Sendhil Mullainathan. How much should we trust differences-in-differences estimates? *Quarterly Journal of Economics*, 119(1):249–275, 2004.
- Gordon Burch, Robert Moakler, Brett R. Gordon, Poppy Zhang, and Shawndra Hill. Characterizing and minimizing divergent delivery in Meta advertising experiments. *Working paper, arXiv:2508.21251*, 2025.
- A. Colin Cameron, Jonah B. Gelbach, and Douglas L. Miller. Bootstrap-based improvements for inference with clustered errors. *Review of Economics and Statistics*, 90(3):414–427, 2008.
- Russell Davidson and Emmanuel Flachaire. The wild bootstrap, tamed at last. *Journal of Econometrics*, 146(1):162–169, 2008.
- Alan S. Gerber and Donald P. Green. *Field Experiments: Design, Analysis, and Interpretation*. W. W. Norton, 2012.
- Brett R. Gordon, Florian Zettelmeyer, Neha Bhargava, and Dan Chapsky. A comparison of approaches to advertising measurement: Evidence from big field experiments at Facebook. *Marketing Science*, 38(2):193–225, 2019.
- Donald P. Green, Shang E. Ha, and John G. Bullock. Enough already about “black box” experiments: Studying mediation is more difficult than most scholars suppose. *Annals of the American Academy of Political and Social Science*, 628(1):200–208, 2010.
- James J. Heckman and Rodrigo Pinto. Econometric mediation analyses: Identifying the sources of treatment effects from experimentally estimated production technologies with unmeasured and mismeasured inputs. *Econometric Reviews*, 34(1–2):6–31, 2015.
- Kosuke Imai, Luke Keele, and Dustin Tingley. A general approach to causal mediation analysis. *Psychological Methods*, 15(4):309–334, 2010a.
- Kosuke Imai, Luke Keele, and Teppei Yamamoto. Identification, inference and sensitivity analysis for causal mediation effects. *Statistical Science*, 25(1):51–71, 2010b.

- Kosuke Imai, Dustin Tingley, and Teppei Yamamoto. Experimental designs for identifying causal mechanisms. *Journal of the Royal Statistical Society, Series A*, 176(1):5–51, 2013.
- Basileal Imana, Aleksandra Korolova, and John Heidemann. Apparent algorithmic discrimination and real-time algorithmic learning in digital search advertising. *Working paper, arXiv:2501.00xxx*, 2025.
- Anja Lambrecht and Catherine Tucker. Algorithmic bias? An empirical study of apparent gender-based discrimination in the display of STEM career ads. *Management Science*, 65(7):2966–2981, 2019.
- Winston Lin. Agnostic notes on regression adjustments to experimental data: Reexamining Freedman’s critique. *Annals of Applied Statistics*, 7(1):295–318, 2013.
- John A. List, Azeem M. Shaikh, and Yang Xu. Multiple hypothesis testing in experimental economics. *Experimental Economics*, 22(4):773–793, 2019.
- Regina Y. Liu. Bootstrap procedures under some non-i.i.d. models. *Annals of Statistics*, 16(4):1696–1708, 1988.
- Jens Ludwig, Jeffrey R. Kling, and Sendhil Mullainathan. Mechanism experiments and policy evaluations. *Journal of Economic Perspectives*, 25(3):17–38, 2011.
- James G. MacKinnon and Halbert White. Some heteroskedasticity-consistent covariance matrix estimators with improved finite sample properties. *Journal of Econometrics*, 29(3):305–325, 1985.
- James G. MacKinnon, Morten Ørregaard Nielsen, and Matthew D. Webb. Cluster-robust inference: A guide to empirical practice. *Journal of Econometrics*, 232(2):272–299, 2023.
- S. C. Matz, M. Kosinski, G. Nave, and D. J. Stillwell. Psychological targeting as an effective approach to digital mass persuasion. *Proceedings of the National Academy of Sciences*, 114(48):12714–12719, 2017.
- Jerzy Neyman. On the application of probability theory to agricultural experiments. Essay on principles. Section 9. *Statistical Science*, 5(4):465–472, 1990. Translation of Neyman (1923).
- Judea Pearl. Direct and indirect effects. In *Proceedings of the Seventeenth Conference on Uncertainty in Artificial Intelligence (UAI)*, pages 411–420. Morgan Kaufmann, 2001.
- James M. Robins. Semantics of causal DAG models and the identification of direct and indirect effects. In Peter J. Green, Nils Lid Hjort, and Sylvia Richardson, editors, *Highly Structured Stochastic Systems*, pages 70–81. Oxford University Press, 2003.
- James M. Robins and Sander Greenland. Identifiability and exchangeability for direct and indirect effects. *Epidemiology*, 3(2):143–155, 1992.

- Joseph P. Romano and Michael Wolf. Stepwise multiple testing as formalized data snooping. *Econometrica*, 73(4):1237–1282, 2005.
- Donald B. Rubin. Estimating causal effects of treatments in randomized and nonrandomized studies. *Journal of Educational Psychology*, 66(5):688–701, 1974.
- Till Speicher, Muhammad Ali, Giridhari Venkatadri, Filipe Nunes Ribeiro, George Arvanitakis, Fabrício Benevenuto, Krishna P. Gummadi, Patrick Loiseau, and Alan Mislove. Potential for discrimination in online targeted advertising. In *Conference on Fairness, Accountability and Transparency (FAT*)*, pages 5–19, 2018.
- Catherine E. Tucker. Social networks, personalized advertising, and privacy controls. *Journal of Marketing Research*, 51(5):546–562, 2014.
- Tyler J. VanderWeele. *Explanation in Causal Inference: Methods for Mediation and Interaction*. Oxford University Press, 2015.
- Chien-Fu Jeff Wu. Jackknife, bootstrap and other resampling methods in regression analysis. *Annals of Statistics*, 14(4):1261–1295, 1986.